X-ray diffraction study of laser-driven solid-state diffusional mixing and new phase formation in Ni-Pt multilayers

B. G. Kelly, A. Loether, K. M. Unruh, and M. F. DeCamp
Department of Physics and Astronomy, University of Delaware, Newark, Delaware 19716, USA

A. D. DiChiara
Advanced Photon Source, Argonne National laboratory, Argonne, Illinois 60439, USA
(Received 17 August 2016; revised manuscript received 6 January 2017; published 1 February 2017)

An *in situ* optical pump and x-ray probe technique has been utilized to study photoinitiated solid-state diffusion in a Ni-Pt multilayer system. Hard x-ray diffraction has been used to follow the systematic growth of the NiPt alloy as a function of laser intensity and total energy deposited. It is observed that new phase growth can be driven in as little as one laser pulse, and that repeated photoexcitation can completely convert the entire multilayer structure into a single metallic alloy. The data suggest that lattice strain relaxation takes place prior to atomic diffusion and the formation of a NiPt alloy.

DOI: 10.1103/PhysRevB.95.064301

Understanding the forces that drive atomic motion has long been of interest for a variety of fields, ranging from studies of structural phase transformations to chemical reactions. For example, diffusional mixing in bimetallic systems can lead to the production of new phases and alloys that can have useful electromagnetic and catalytic properties [1,2]. Studies that reveal atomic motion during solid-state mixing can lead to a fundamental understanding behind the production of these novel molecular structures.

In many cases compositional gradients and thermal excitation are the main factors that drive atomic transport. For example, studies of thermal activation in nickel-platinum systems have shown that the atomic diffusion constant is 10^{-13}–10^{-10} cm^2/s over a temperature range of 1200–1600 K [3]. In addition, in systems with planar symmetry, the amount of mixed phase material can be described by a simple power law as a function of time [4]:

$$W = W_o + At^n \tag{1}$$

whereby in diffusion limited systems, n=0.5 as described by Fick's Law. However, in systems with steep compositional and/or thermal gradients, it has been shown that the growth of new phase material does not follow a standard diffusion rate model, especially at early times where $n \sim 1$ [5]. Therefore experimental methods that can simultaneously measure the composition and growth of this new mixed phase are desirable to fully characterize the atomic motion.

X-ray diffraction (XRD) scattering methods are the preeminent tool for structural refinement of systems at the nanoscale. In particular, the angular positions of diffraction peaks are governed by the Laue equation:

$$\vec{G} = \vec{k}_o - \vec{k}_i \tag{2}$$

where $\vec{G}$ is the reciprocal-lattice vector associated with the material composition and $\vec{k}_{i,o}$ are the incident and output x-ray wave vectors. Accurate measurement of the scattering vector allows one to reconstruct the chemical composition of condensed phase materials [6]. Furthermore, when integrated with simple thermal excitation, the kinetics of compositional changes can be directly revealed [7]. For example, as early as 1940, it was shown that XRD methods can be used to study diffusional mixing in solids [8]. These studies, however, have primarily been limited to the quasistatic regime, i.e., where the sample is in thermal equilibrium with the environment. Under these conditions many different diffusional pathways within the complex energy landscape are sampled, making it difficult to identify the specific forces that drive the atomic motion.

In contrast, picosecond optical excitation can provide a nearly instantaneous pulse of energy to the atomic lattice which in turn drives the system to a highly nonequilibrium state. In particular, when intense optical radiation interacts with a metal, a large number of "hot electrons" are generated within the optical penetration depth of the material. This electron plasma very rapidly diffuses through the metal and thermalizes with the atomic lattice on picosecond time scales [9,10]. Pulsed laser systems can generate temperature jumps in solids well in excess of 1000 K [11–13]. Previous studies integrating pulsed laser excitation with small angle x-ray scattering techniques have provided direct evidence of optically driven atomic diffusion solid-state systems [14,15]. However, small angle x-ray scattering is only representative of the modulation in the composition profile of a multilayer film, and is not very sensitive to the molecular composition of the newly formed phase.

In this paper, optical pump and wide angle XRD measurements have been used to study the *in situ* photoinduced atomic diffusion and alloy formation in a Pt-Ni multilayer film. This prototypical system was chosen because of its simple structural phase diagram [16] and well-separated lattice parameters of the individual atomic species as well as the metallic alloy. The use of wide angle x-ray scattering allows the reconstruction of the composition profile of the new phase formation as well as revealing the lattice strains within the multilayer structure.

For the experiments described below, a metallic multilayer system was grown via sputtering on a standard silicon wafer. The multilayer was composed of 11 (10) layers of Ni (Pt), each approximately 5-nm thick. Experiments were performed at the BioCARS undulator beamline (sector 14-ID) at the Advanced Photon Source (APS) at Argonne National Laboratory [17], whereby 48 000 12.0-keV hard x-ray pulses illuminated the sample at a fixed incident angle of approximately 5 deg (see

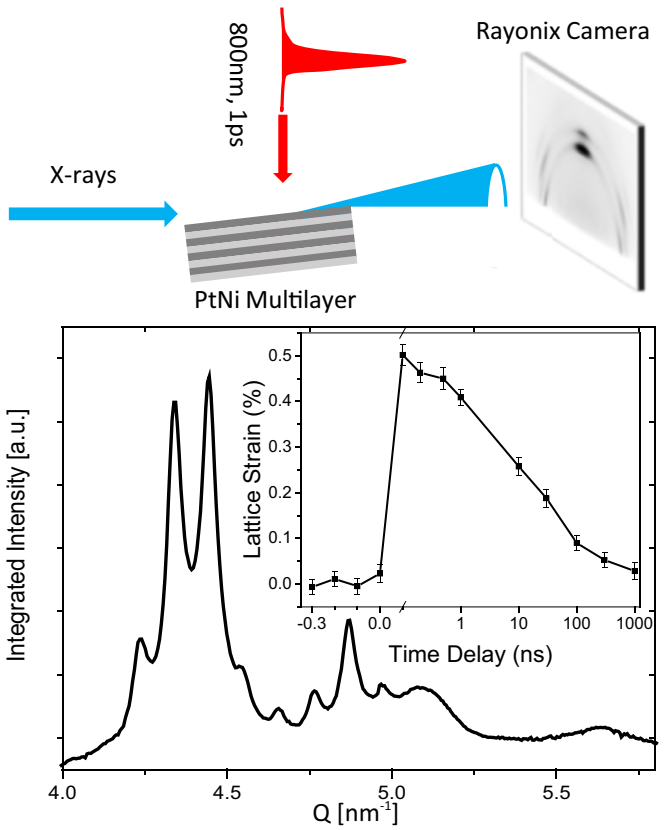

FIG. 1. Top: Experimental setup. Bottom: Complete radial integration of the two-dimensional diffraction pattern of the as-prepared sample. Inset: Time-resolved x-ray-diffraction measurement of a laser excited NiPt alloy.

Fig. 1). At this angle and x-ray energy, the average attenuation depth within the sample was approximately 300 nm, therefore the x rays are able to sample the entire multilayer structure with limited attenuation. The resulting two-dimensional XRD pattern was collected by a Rayonix MX340-HS camera. The output scattering vector was calibrated using a standard CeO_2 polycrystalline sample. Background dark images and transient hot pixels (generated by external electrical and/or cosmic sources) were manually removed from each two-dimensional diffraction image.

Upon a simple radial integration of the entire diffracted signal (see Fig. 1), we observe several diffraction peaks associated with the sample. In the diffraction region associated with the 111 family of diffraction planes of Pt and Ni (4.1 to 5.0 nm^{-1}) "fast" periodic modulations in the diffraction intensity are clearly visible consistent with the existence of a multilayer structure. In addition, we observe two broad peaks centered approximately at 5.1 and 5.65 nm^{-1}, consistent with the (200) peaks of Pt and Ni, respectively. The lack of periodic modulations around these peaks suggests that the multilayer was grown in a direction parallel to the (111) diffraction planes of Pt and Ni.

In an effort to deconvolve the multilayer diffraction signal with the atomic composition, each background subtracted diffraction image was radially integrated into 60-deg ϕ bins such that the off-axis (200) and (111) diffraction planes (located at $|\phi| > 30^\circ$) could be isolated from the "on-axis" diffraction patterns ($\phi \sim 0^\circ$). As the off-axis directions have limited sensitivity to the reciprocal-lattice vector of the multilayer, the x-ray scattering is dominated by the material composition. In contrast, the on-axis diffraction patterns include significant contributions from the modulations of the chemical composition associated with the multilayer, thereby suppressing the signal from individual atomic layers. However, the modulation depth within the observed multilayer diffraction pattern is highly sensitive to both the periodicity and composition gradient at the boundary interfaces, providing a method to detect small changes in atomic composition at the boundary interfaces. Therefore analyzing both the on- and off-axis diffraction contributions simultaneously can provide complementary information on the chemical composition of the sample. Prior to peak fitting, an additional background subtraction was performed on each radial integration. For each series of laser excitations, three independent measurements on different locations on the crystal surface were performed.

Optical pump pulses were generated by a Spectra Physics Spitfire laser system, which delivered ~1-ps 800-nm pulses of radiation to the sample. The laser was incident on the metallic surface approximately parallel to the surface normal, providing a quasihomogenous laser intensity over the entire x-ray interaction region. The optical intensity was controlled via a neutral density filter. At 800 nm, the optical absorption depth (reflectivity) of Ni and Pt is 14.5 nm (68%) and 12.8 nm (71%), respectively [18], implying that the optical radiation only penetrated the first few multilayer periods, and that approximately 30% of the incident optical energy was absorbed into the multilayer structure. Time-resolved XRD experiments of a laser annealed PtNi alloy film upon exposure of a 50-mJ/cm^2 optical pulse (see Fig. 1 inset) indicate that the ultrafast laser excitation provides a quasiinstantaneous lattice strain within the sample. Simple extrapolations using linear thermal expansion imply that the laser imparts a temperature rise in excess of 450 K within the sample with a characteristic decay time of 20–50 ns, consistent with thermal diffusion to the environment [19–21]. While time-resolved XRD measurements were possible on the annealed alloy, due to the irreversible structural changes within the as-grown sample, time-resolved measurements were not possible given the size of the sample and lack of precise rastering capabilities during the current experiment.

In Fig. 2, the two-dimensional XRD patterns and resulting on- and off-axis radial integrations are shown for the as-prepared multilayer sample. Direct inspection of the XRD patterns reveals that the deposited multilayer is preferentially grown such that the (111) lattice planes are parallel to the surface of the substrate, i.e., only the (111) family of diffraction peaks is observed along $\phi = 0^\circ$.

To reconstruct the composition of the sample, the measured XRD patterns around $\phi = 0^\circ$ were compared directly to simple one-dimensional kinematic calculations of the scattered intensity profile [22–24]. Fits reveal that the as-grown sample possessed approximately 18.5(6) and 25.5(7) atomic planes of Pt and Ni, respectively, in each metallic layer, with approximate lattice parameters of 0.397 and 0.3535 nm for the Pt and Ni, respectively, significantly larger than accepted

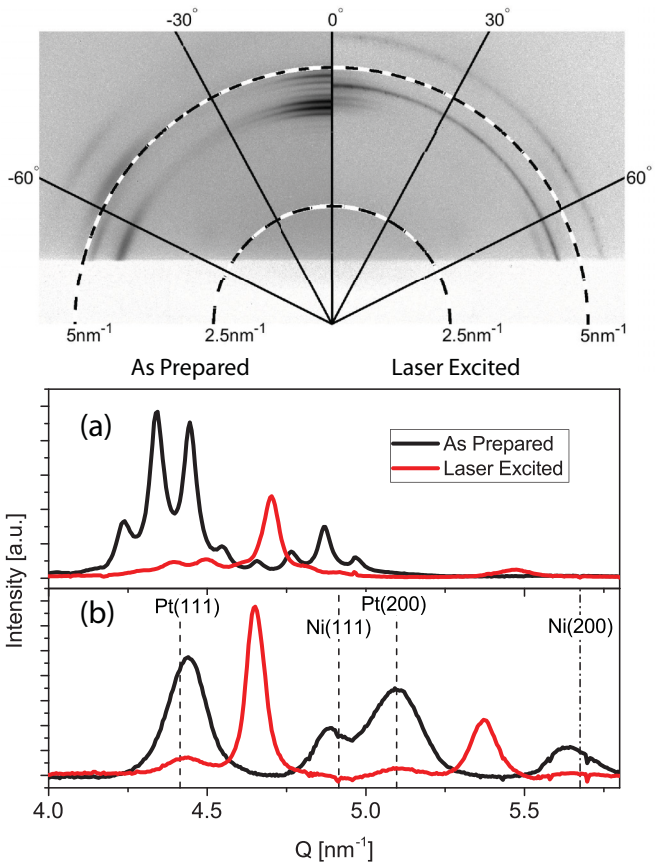

FIG. 2. Measured XRD pattern of Ni-Pi multilayer. Top: 2D diffraction pattern of the as-prepared (left) and laser excited (right) sample. Dashed lines represent equal magnitude in the scattering vector. Solid lines are the "ϕ" angle with respect to the surface normal of the sample. Bottom: Radial integrations of the 2D diffraction pattern at $\phi = 0°$ (top) and $|\phi| > 30°$ (bottom) for the as-prepared sample (black) and upon exposure to three 250-mJ/cm^2 laser pulses (red). Dashed lines represent scattering vectors associated with bulk Pt and Ni.

bulk values for the constituent metals (0.3924 and 0.3524 nm, respectively).

Fitting the off-axis (111) family of diffraction peaks to a series of Gaussian curves, the as-grown sample was determined to be composed of 59(1)% Ni and 39(1)% Pt consistent with the analysis above. The fits indicated that the atomic lattice parameters in the off-axis direction are 0.39041(2) and 0.35358(14) nm for the Pt and Ni, respectively, indicating that the system is under significant asymmetric lattice strain prior to laser exposure.

Following exposure of only three laser pulses at an optical fluence of 250 mJ/cm^2, dramatic changes in the XRD patterns are apparent (see Fig. 2). Under these conditions, if we assume that the imparted temperature rise in the sample is proportional with an incident laser intensity, the material will have experienced a temperature jump in excess of 2200 K, well above the reported melting temperature of both Pt and Ni. The diffraction intensity is almost eliminated in both the atomic Ni (111) and Pt (111) peaks. In addition, there is a set of new

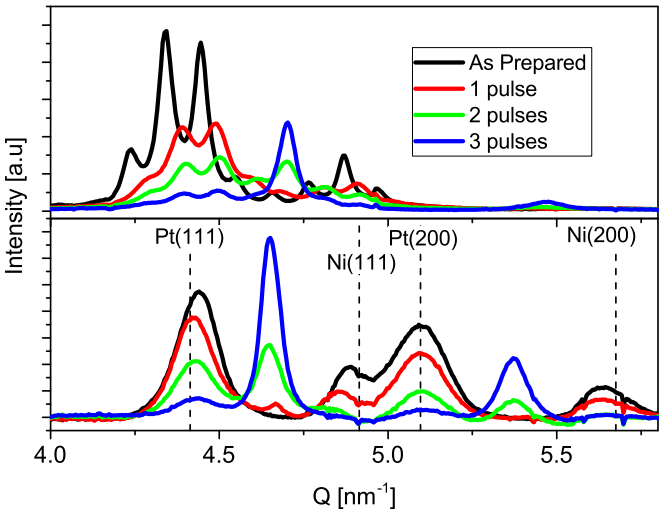

FIG. 3. XRD patterns of the as-prepared sample (black), after one laser pulse (red), after two laser pulses (green), and after three laser pulses (blue) at a laser fluence of 250 mJ/cm^2. Top: $\phi = 0°$. Bottom: $|\phi| > 30°$. Dashed lines represent scattering vectors associated with bulk Pt and Ni.

diffraction peaks at $Q \sim 4.65$ and 5.35 nm^{-1}, consistent with reported lattice parameters of PtNi alloys [25].

To follow the formation of the new mixed phase, XRD measurements were taken as a function of laser exposure (see Fig. 3). After a single laser pulse, both the Pt (111) and Ni (111) multilayer peaks have systematically shifted to larger scattering vectors. In addition, the diffraction contrast associated with the multilayer periodicity is significantly reduced, consistent with atomic diffusion across the Pt-Ni boundary. However, as the diffusion has not been completed, the multilayer diffraction pattern dominates the on-axis contribution, thereby suppressing the diffraction contribution due to the composition of the alloy. In the off-axis directions, the scattering vectors of the Pt (111) and Ni (111) peaks shift and a clear PtNi (111) diffraction peak is observed.

Further laser excitation displays the growth of both PtNi (111) and (200) peaks, and after only three laser pulses, 93(2.5)% of the sample has been converted to the new metallic phase. Subsequent laser pulses do not appear to convert any additional material to the alloy, suggesting that atomic diffusion is completed. Concurrent XRD patterns along the $\phi = 0°$ direction include the formation of not only the PtNi (111) peak but a significantly suppressed PtNi (200) peak as well, suggesting that the alloy formation is slightly amorphous.

Upon further inspection, the scattering vector of the PtNi alloy peaks is dependent on the ϕ angle, suggesting that the new phase has formed under significant static strain. After an additional ten laser pulses (not shown) the peaks converge to approximately the same scattering vector, suggesting that repeated laser exposure leads to a more isotropic alloy. However, under these conditions there is significant visible surface damage to the sample as well as a global loss of XRD intensity, consistent with a large amount of material being removed by the laser excitation.

To minimize laser ablation and to more closely follow the growth of the new metallic phase, the optical fluence was

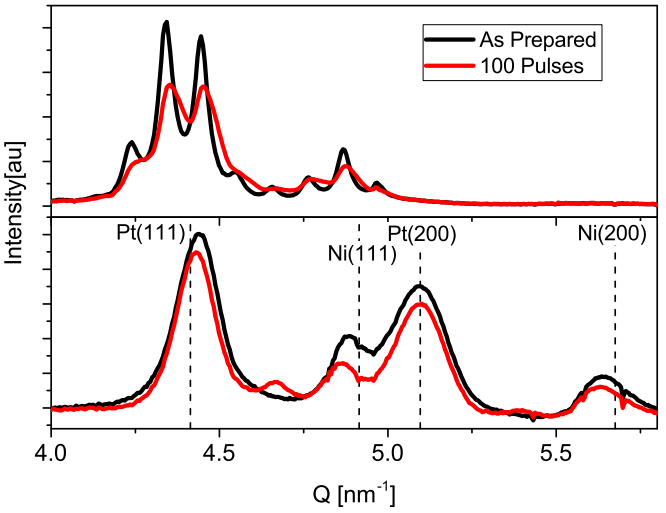

FIG. 4. XRD patterns of the as-prepared sample (black) and following laser excitation of 100 mJ/cm^2 (red). Top: $\phi = 0°$. Bottom: $|\phi| > 30°$. Dashed lines represent scattering vectors associated with bulk Pt and Ni.

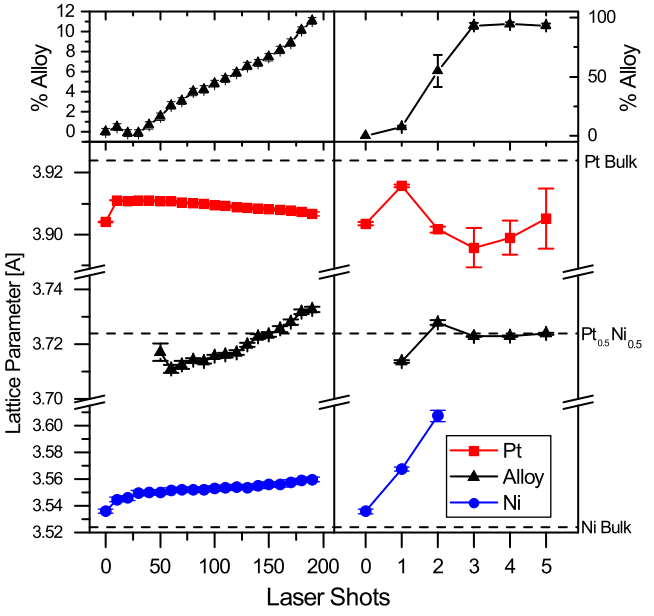

FIG. 5. Results of nonlinear least-square fittings to measured data as a function of laser excitation. Left column: Incident laser fluence 100 mJ/cm^2. Right column: Incident laser fluence 250 mJ/cm^2. Top row: Alloy percentage. Bottom row: Retrieved lattice parameters of Pt (red), Ni (blue), and PtNi alloy (black). Dashed lines represent scattering vectors associated with bulk Pt and Ni. Error bars represent standard errors from fits.

reduced to 100 mJ/cm^2 (see Fig. 4). At this laser intensity, we estimate that the laser provided a temperature rise on the sample of about 900 K, below the melting temperature of Pt or Ni. Upon repeated laser exposure, the total integrated XRD intensity did not change over 200 laser pulses, suggesting that optical ablation was minimized. Like the data at higher laser intensities, after 100 laser pulses, a Pt and Ni lattice shift is observed and a clear PtNi (111) XRD peak is formed in the off-axis scattering directions. In the $\phi = 0°$ direction, like above, there is no direct evidence of the formation of a new phase due to the residual multilayer periodicity; however, the diffraction contrast associated with the multilayer periodicity is reduced, consistent with atomic migration across the Pt-Ni boundary.

Gaussian peak fitting of the (111) family of peaks in the off-axis directions reveals the structural changes in detail as a function of laser exposure (see Fig. 5). For the 100-mJ/cm^2 excitation, after only ten laser pulses, the Pt and Ni lattice expands 0.17 and 0.25%, respectively, without any evidence for alloy formation. After 50 laser pulses, XRD peaks associated with the metallic alloy appear, which grow in amplitude approximately linearly with laser excitation, reaching greater than 10% conversion in 200 laser pulses. During the repetitive laser exposure the measured Pt lattice parameter is slowly reduced over several hundred laser pulses, while the Ni lattice continues to expand another 0.3%. The lattice parameter of the alloy also changes linearly with laser exposure growing from 0.37110(18) to 0.37325(12) nm in the first 200 laser shots, consistent with changes in chemical concentration in the alloy layer.

In the 250-mJ/cm^2 data, after a single laser pulse the Pt and Ni lattice parameters have increased 0.3 and 0.9%, respectively, while $7.5 \pm 1\%$ of the sample converted to the alloy. The second laser pulse leads to a compression of the Pt and a further expansion of the Ni lattice in conjunction with a significant increase in alloy production. Finally, after three laser pulses, the sample is over 93% in the alloy state. Like above, the lattice parameter of the alloy peak appears to change with the growth of the new phase. In particular, after one laser pulse the peak position is consistent with a nickel rich alloy, and after repeated laser excitation the resulting lattice parameter is consistent with an equal mixture of Ni and Pt. Along the $\phi = 0°$ direction, the Pt lattice parameter has compressed by $\sim$2%, and after two laser shots the XRD pattern is composed of a superposition of the multilayer structure with metallic alloy state, suggesting that the new mixed phase was formed nonuniformly as a function of material depth. After three lasers shots, the XRD pattern is dominated by the metallic alloy.

The apparent correlation between the shifting of the lattice parameters with appearance of the alloy state suggests a diffusional pathway for the growth of the new phase. In particular, there are several sequential and correlated events that occur during the mixing process: (1) the rapid change of both Pt and Ni lattice parameters, (2) the simultaneous shift in the Ni lattice peak and the production of the PtNi alloy, and (3) relaxation of strain in the PtNi alloy.

The initial change in the Pt and Ni lattice parameters prior to any significant new phase formation suggests that a reduction in lattice strain precedes atomic migration across the interface. As lattice strain is dependent on the atomic defect concentration [26] and the lattice parameter of alloys can be described by Vegard's law [27], the subsequent slow evolution of the Pt lattice parameters to smaller values and the rapid migration of the Ni and PtNi lattice parameters to larger values are consistent with Pt atoms preferentially migrating into the Ni rich areas. In addition, data from excitation at 100 mJ/cm^2 demonstrate a linear progression

of alloy formation as a function of laser exposure, consistent with linear power law as described by Eq. (1). Following the above-mentioned diffusional steps, the observed residual ϕ-dependent strain in the resultant alloy suggests that even after atomic diffusion has been "completed" atomic mixing is still ongoing, producing a more isotropic alloy upon repeated laser exposure.

In conclusion, we have measured the *in situ* growth of a metallic alloy driven by intense optical radiation. The data suggest that photodriven structural changes are mediated by a multistep process, which includes atomic lattice relaxation followed by atomic migration. Ongoing integration of precise, and repeatable, lateral control over the sample position will allow future experiments to explore this atomic motion using time-resolved x-ray diffraction technique to explore the motion at both the atomic scale and the subnanosecond time scales.

We would like to thank John Xiao for growing the sample, Robert Henning for technical support, and James MacDondald for useful discussions. This work was supported by the NSF under Grant No. DMR1410076. Use of the Advanced Photon Source was supported by the U.S. Department of Energy, Basic Energy Sciences, Office of Science, under Contract No. DE-AC02-06CH11357. Use of the BioCARS Sector 14 was also supported by the National Institutes of Health, National Institute of General Medical Sciences Grant No. R24GM111072.

[1] Q. Zhang, I. Lee, J. B. Joo, F. Zaera, and Y. Yin, Acc. Chem. Res. **46**, 1816 (2013).
[2] Z. Cui, F. Gao, and J. Qu, J. Mech. Phys. Solids **61**, 293 (2013).
[3] M. S. A. Karunaratne and R. C. Reed, Acta Mater. **51**, 2905 (2003).
[4] Z. Mei, A. Sunwoo, and J. Morris, Metall. Trans. A **23**, 857 (1992).
[5] U. Gösele and K. N. Tu, J. Appl. Phys. **53**, 3252 (1982).
[6] J. I. Langford and D. Louër, Rep. Prog. Phys. **59**, 131 (1996).
[7] W.-H. Wang, H. Y. Bai, M. Zhang, J. H. Zhao, X. Y. Zhang, and W. K. Wang, Phys. Rev. B **59**, 10811 (1999).
[8] J. DuMond and J. Youtz, J. Appl. Phys. **11**, 357 (1940).
[9] C. Thomsen, J. Strait, Z. Vardeny, H. J. Maris, J. Tauc, and J. J. Hauser, Phys. Rev. Lett. **53**, 989 (1984).
[10] C. Thomsen, H. T. Grahn, H. J. Maris, and J. Tauc, Phys. Rev. B **34**, 4129 (1986).
[11] A. M. Lindenberg, I. Kang, S. L. Johnson, T. Missalla, P. A. Heimann, Z. Chang, J. Larsson, P. H. Bucksbaum, H. C. Kapteyn, H. A. Padmore, R. W. Lee, J. S. Wark, and R. W. Falcone, Phys. Rev. Lett. **84**, 111 (2000).
[12] L. Guo, S. L. Hodson, T. S. Fisher, and X. Xu, J. Heat Transfer **134**, 042402 (2012).
[13] B. Salatić, S. Petrović, D. Peruško, M. Čekada, B. Jelenković, and D. Pantelić, Opt. Quantum Electron. **48**, 314 (2016).
[14] E. Majkova, S. Luby, M. Jergel, Y. Chushkin, E. Anna, A. Luches, M. Martino, P. Mengucci, G. Majni, Y. Kuwasawa, and S. Okayasu, Appl. Surf. Sci. **208–209**, 394 (2003).
[15] E. D'Anna, S. Luby, A. Luches, E. Majkova, and M. Martino, Appl. Phys. A **56**, 429 (1993).
[16] P. Nash and M. F. Signleton, Bulletion of Alloy Phase Diagrams **10**, 258 (1989).
[17] T. Graber, S. Anderson, H. Brewer, Y.-S. Chen, H. Cho, N. Dashdorj, R. Henning, I. Kosheleva, G. Macha, M. Meron, R. Pahl, Z. Ren, S. Ruan, F. Schotte, V. Srajer, P. Viccaro, F. Westferro, P. Anfinrud, and K. Moffat, J. Synchrotron Radiat. **18**, 658 (2011).
[18] A. D. Rakić, A. B. Djurišić, J. M. Elazar, and M. L. Majewski, Appl. Opt. **37**, 5271 (1998).
[19] Y. M. Sheu, S. H. Lee, J. K. Wahlstrand, D. A. Walko, E. C. Landahl, D. A. Arms, M. Reason, R. S. Goldman, and D. A. Reis, Phys. Rev. B **78**, 045317 (2008).
[20] M. Highland, B. C. Gundrum, Y. K. Koh, R. S. Averback, D. G. Cahill, V. C. Elarde, J. J. Coleman, D. A. Walko, and E. C. Landahl, Phys. Rev. B **76**, 075337 (2007).
[21] D. A. Walko, Y.-M. Sheu, M. Trigo, and D. A. Reis, J. Appl. Phys. **110**, 102203 (2011).
[22] E. E. Fullerton, I. K. Schuller, H. Vanderstraeten, and Y. Bruynseraede, Phys. Rev. B **45**, 9292 (1992).
[23] Y. Ishibashi, N. Ohashi, and T. Tsurumi, Jpn. J. Appl. Phys. **39**, 186 (2000).
[24] E. Zolotoyabko, Y. Finkelstein, M. Blumina, and D. Fekete, Physica B **221**, 487 (1996).
[25] U. Kumar, K. G. Padmalekha, P. K. Mukhopadhyay, D. Paudyal, and A. Mookerjee, J. Magn. Magn. Mater. **292**, 234 (2005).
[26] P. H. Dederichs, J. Phys. F **3**, 471 (1973).
[27] A. R. Denton and N. W. Ashcroft, Phys. Rev. A **43**, 3161 (1991).